The Efficiency Characterization of Germanium Detectors at Energies less than 45 keV -- 10479

K.E. Morris[1], W.F. Mueller[1], P. Blanc[1], F. Bronson[1], S. Croft[1], M.B. Field[1], D.R. Nakazawa[1], R. Venkataraman[1] and H. Zhu[1]
[1]Canberra Industries Inc., 800 Research Parkway, Meriden, CT 06450, USA

ABSTRACT

With the availability of large-volume thin-window germanium detectors, it is possible to routinely measure very low-energy (<45 keV) gamma and X-rays while maintaining good sensitivity for high-energy gamma rays. The effective calibration of such detectors down to these low energies is often problematic or infeasible because of the lack of calibrated sources or knowledge of the source form factor. With the aid of a semi-analytical mathematical approach for modeling the absolute efficiency of the germanium detector, it is possible to have a low-energy efficiency calibration that is relatively accurate. Combined with algorithms to calculate the transmission corrections factors for a wide range of user-definable geometries and materials, this approach is also versatile enough to be used in many routine applications. We discuss the challenge of gamma-ray transmission calculation for common low Z container and matrix materials, and discuss the transmission calculations performed by mathematical efficiency models. We present the results of a comparison of the mathematically-modeled transmission fractions to a set of measured transmission fractions in the range of 13-662 keV, and we demonstrate the accuracy of the transmission correction factors of mathematical calibrations to source-based measurements. We found agreement within 1% for all materials at energies greater than 45 keV. For energies less than 45 keV down to 13.9 keV, we reproduce measured values transmission fractions to within 10%, with the exception of glass material at 13.9 keV, which was 25% (619%, 1sd).

INTRODUCTION

Mathematical efficiency calibrations can provide a viable alternative to traditional source-based efficiency calibration of gamma-ray detectors [1, 2, 3]. Most traditional approaches allow measurement of efficiencies down to about 45 to 60 keV, but recent advances have allowed the extension of mathematical efficiency calibrations down to as low as 10 keV [4], which is difficult to achieve using a source-based approach. A low-energy efficiency calibration can be useful, for example, in the monitoring and quantification of plutonium surface contamination. Plutonium has significant X-ray radiation in the 14 to 20 keV region with yields about three orders of magnitude greater than the gamma-ray yields. Thus, X-ray quantification can significantly reduce assay times in surface contamination analysis. Another application is the ability to perform analysis of nuclides which emit only low-energy gamma rays such as I-125, which is a common medical isotope, and I-129, which, as a long-lived byproduct of uranium and plutonium fission, is of interest in the monitoring and measuring the effects of weapons

testing and fast fission reactors. In other scenarios, the ability to analyze X-rays and lower energy gamma rays may help in nuclide identification, especially when a sample has nuclides of many interfering lines. For example, in high-efficiency counting geometries it is possible for certain nuclides to have cascade (or true coincidence) summing losses with X-rays or low energy gamma rays. If uncorrected, true coincidence summing will systematically bias counts in a specified full energy peak. Common nuclides that have potential for such biases include Co-60, Y-88, Ce-139, Eu-152, Cs-134, and Ba-133. Quantification of efficiency down to low 10 keV allows for the correction of true coincidence summing between two high-energy gamma rays as well as the true coincidence summing of a gamma ray with X-rays and low-energy gamma rays [5,6].

In this study, we utilize Canberra Industries' ISOCS/LabSOCS mathematical efficiency calibration approach [3]. This approach uses knowledge of detector construction and comparison to well-defined measurements of NIST-traceable sources to create a validated MCNP (Monte Carlo N-Particle) model of the radiation detector. This model is then used to compute point efficiencies in a spatial grid surrounding the detector. This is supplied as a detector characterization file, which defines the efficiency at all points in space around the detector out to 500 meters. After a user defines a geometry in the user-interface, the software then divides the active region of the source into many voxels and the detector surface into many pixels. For each voxel-pixel pair, the software has two steps. The first is to access and determine from the detector characterization file the vacuum efficiency at that voxel location. The second is to determine the effective attenuation for all materials between the sample voxel and the detector pixel.   The vacuum efficiency for each voxel-pixel pair is corrected for attenuation and integrated over the entire active volume of the source geometry.

In Ref. [4], the results of ISOCS comparisons to measured point sources of various spatial positions at low energies in air are presented, addressing the accuracy of the first aspect of vacuum (or in this case near-vacuum) efficiencies. In this paper we focus on the accuracy of attenuation calculations performed using ISOCS/LabSOCS software at low energies.

Attenuation is very significant at these low energies. If the sample being measured is thick, only photons from the outer layer emerge from the sample. And the sample must be contained somehow, which can also be a significant attenuator. For example, it can be demonstrated that 3 mm of plastic, as may be encountered at the thicker base of many bottles, will reduce the efficiency for a sample by 25% at 20 keV and as much as 85% at 10 keV. In this paper we focus on materials that are likely to be encountered in common sample containers and as sample matrices.

METHODOLOGY

Experimentally, the overall gamma ray transmission of a geometry is adequately represented by Beer's law ($e^{-\mu t}$, when t is the total thickness and μ is the gamma ray attenuation coefficient), only when the solid angle is small. This may occur in a tightly collimated geometry or for large source-detector distances, where the path lengths through absorber materials can be approximated by only a single value. These geometries are not representative of many commonly used situations, when the diameter of the detector subtends a large solid angle. Therefore no single path length represents the effective "thickness" of the absorber. Using a multi-ray approach, the ISOCS/LabSOCS software calculates the attenuation for multiple paths to determine the true attenuation of an absorber. The algorithms calculate the path lengths of the rays and fold it with published cross sections [7] to correct efficiency in each spatial region for attenuation effects. The algorithms are energy dependent and therefore successfully account for discontinuities of cross sections introduced by K- and L-shell absorption edges.

Verification of ISOCS/LabSOCS attenuation corrections is geometry-dependent. To best determine the accuracy of the linear attenuation coefficient, the ideal geometry would be a tightly collimated source attenuated through a planar and infinite width absorber perpendicular to the source beam. This would make the effective thickness of the absorber the same as that of the physical thickness. However, in the majority of typical measurement situations, the source is not tightly collimated. The path length of attenuation is the absorber thickness only in the perpendicular case; for photons emitted at a greater angle but still within the solid angle of the detector, the effective absorber thickness is longer. Also other effects such as coherent scattering, where a gamma ray from a larger angle may be scattered back into the detector without any loss of energy, may occur. While a tightly collimated source with infinite width absorber is the ideal geometry for verifying the linear attenuation coefficient, an uncollimated source better represents a typical measurement geometry and is more valid for verification of attenuation calculations for typical measurement purposes, in geometries which efficiency calibrations are most frequently employed.

MEASUREMENTS

Measurements were performed with two CANBERRA High Purity Germanium (HPGe) Detectors: a Low Energy Planar (LEGe) 20 cm^2 area and 2 cm thick detector and a Reverse Electrode Coaxial (REGe) detector of 50% relative efficiency. Measurements performed with the LEGe were done to gain a good qualitative understanding of the peaks and background of the geometry, while the majority of attenuation measurements were performed with the higher-efficiency REGe detector.

The source used for all comparisons presented in this study is a point source consisting of about 0.5 microcurie each of Am-241 and Cs-137. The source was prepared by Eckert and Ziegler Analytics and certified with a 1% activity uncertainty at 1 standard deviation. It is electro-deposited on a 9 mg/cm^2 plastic disk with a 0.8 mg/cm^2 aluminized Mylar

cover. Sensitivity studies were done to show that the Mylar cover had no significant effect at the energy range of interest.

Am-241 is an appropriate radionuclide source for low-energy studies as it has a multitude of L-shell X-rays in the 14-22 keV region, a low-energy gamma ray at 26.3 keV, and prominent gamma ray at 59.5 keV [8]. Cs-137 decay, meanwhile, has K-shell X-rays in the region of 31 to 38 keV, sufficiently above the Am-241 X-rays and 26.3 keV gamma ray to avoid overlap. Cs-137 emits a highly intense gamma ray at the mid-range energy of 662 keV, providing a suitable reference peak minimally affected by attenuation to monitor unexpected changes in the experimental set-up. A representative energy spectrum is presented in Figure 1.
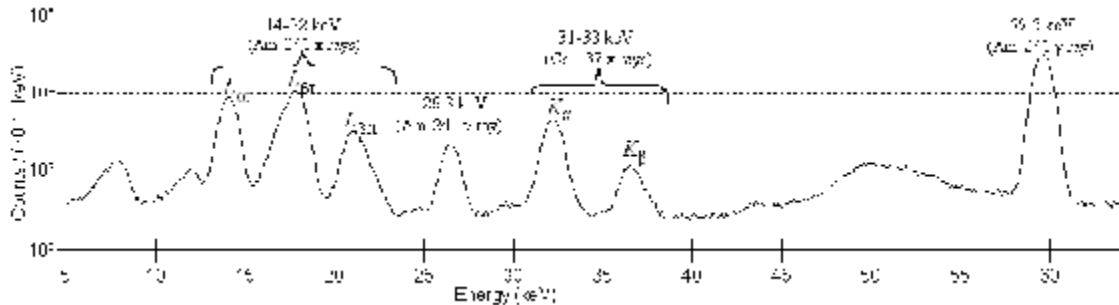
Figure 1. Spectrum from a 50% relative efficiency reverse-electrode high purity germanium detector of an Am-241/Cs-137 point source at a distance of 7cm from the detector. This spectrum spans from 5 to 65 keV, and illustrates the typical resolution and peak structure seen with the majority of measurements. This geometry does not have any attenuating material, other than air, between the source and the detector endcap.

To quantify the uncertainty in the peak fitting methods, spectra were systematically analyzed to determine the variance of different fitting schemes for the complicated X-ray and low-energy gamma ray region. Included in this analysis were spectra demonstrating large effects of build-up, down scatter, and resolution degradation due to significant attenuation. Parameters that were varied include region of interest (ROI) bounds, background functions (linear vs. step), and number of identified peaks within multiplet regions. It was found that on average an 8% variation could be seen for Am-241 X-rays and about a 2% variation for the low-energy Am-241 gamma ray and Cs-137 X-rays.

The geometry used for all test measurements consists of the Am-241/Cs-137 point source placed in a source stand that is secured to the detector endcap. This source stand suspends the source at a distance of 7 cm centered over the detector endface and is calibrated such that the source can be repositioned to within 1mm accurately. This translates into about a 2.8% uncertainty in efficiency. For each material test, two measurement geometries were used: one test geometry with an attenuating material placed between the source and endcap, and one reference geometry in which no intervening materials are present. The observed transmission is then calculated as the ratio of the peak areas for a given full energy peak between an attenuated geometry and the respective reference geometry. Between measurements the source is not repositioned, and uncertainty in source location is not included in final transmission uncertainties.

A selection of materials was used as absorbers, focusing on common container materials used in sample assays. There materials are also believed to be representative of many common sample matrices (water, vegetation, filter paper, foods, biota). Chemical compositions and densities used for modeling and determination of materials' mean free path are provided in Table 1. Chemical compositions were determined from manufacturer's specifications when available and from other standard references, and densities were determined by measurements of the material mass and volume.

Table 1 List of materials used in this study. Included are the material composition and the density and thickness. Please note the material compositions listed are simplified chemical compositions and are not necessarily representative of the materials' chemical structures.

Material	Assumed Composition	Thickness (cm)		Density (g/cc)	
Polycarbonate	$C_{15}H_{16}O_2$	0.300	60.010	1.178	60.136
High Density Polyethylene (HDPE)	C_2H_4	1.280	60.005	0.950	60.010
Nylon	$(CH_2)_8(CONH)_2(H_2O)_2$	0.158	60.005	1.140	60.036
Glass	72.20%(SiO_2) + 14.30%(NaO) + 6.40%(CaO) + 4.30%(MgO) + 1.20% (AlO) + 1.20% (KO) + 0.03%(SO_3) + 0.03% (FeO)	0.120	60.005	2.587	60.022
Delrin	CH_2O	0.162	60.005	1.390	60.045
Rubber	$C_{10}H_{16}S_2$	0.258	60.005	1.082	60.022
Synthetic Rubber Silicone	$(C_6H_5)_2SiO$	0.258	60.005	1.082	60.022

In Figure 2 and Table 2, the observed transmission fraction is presented as a function of fraction of mean free path for each material and energy. Mean free path, ℓ, is defined to be the distance in which the gamma ray intensity is reduced by $1/e$. The mean free path is related to the thickness of the material by its photon scattering cross section (μ/ρ) and density (ρ) by the relationship $\ell = \left(\left[\frac{\mu}{\rho} \right] \rho \right)^{-1}$, where the μ/ρ values are computed from elemental mass attenuation factors tabulated in Ref. [7]. The transmission fraction follows the relationship $T = I/I_0 = e^{-t/\ell}$, where t is the effective thickness of the material. This relationship is represented by the Theoretical Relationship in Figure 2, and it can be seen that the majority of the materials presented demonstrate close agreement to the expected value, both with materials that are slightly attenuating (polycarbonate) and ones that are significantly attenuating (glass). The degree of uncertainty in transmission is listed in Table 2 and is discussed in further detail later on.

This approach demonstrates significant sensitivity to material composition, which is demonstrated in Figure 2 by including two possible chemical compositions of the material Rubber. Synthetic rubber is a complex material that often has various compounds substituted into the matrix during production to yield different desirable physical characteristics, such as chlorine, silicon, and sulfur. According to manufacturer's specifications, the rubber used for this study consisted of low temperature

silicone; however, it is shown that a chemical composition of a common sulfur-based synthetic rubber agrees much closer with the expected transmission behavior. The substantial difference seen here between observed transmission and the expected theoretical trend, which is based on a specified mass attenuation coefficient, may indicate that the assumed material composition is not correct.
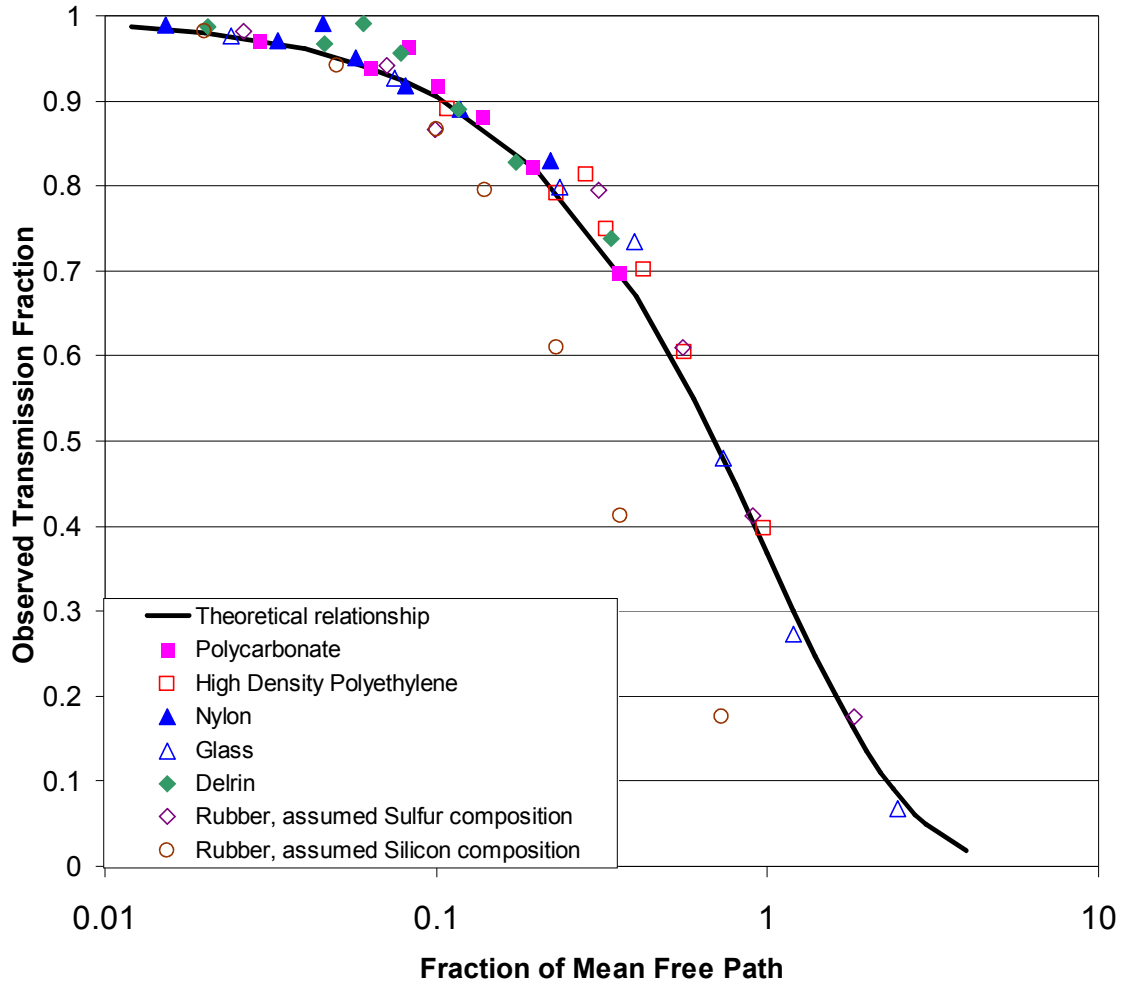
Figure 2 Comparison of the observed material transmission fractions versus the fraction of the mean free path of the absorber material. The Theoretical Relationship illustrated is *Transmission* = exp(- *fraction of mean free path*) and shows the expected behavior of attenuation as the amount of attenuating material increases.

Table 2 Observed Transmission Fraction and Fraction of Mean Free Path of each material. Uncertainty listed includes counting statistics and fitting variances. Fraction of mean free path is calculated using knowledge of material's composition, measured thickness and density, and known peak energy.

Energy (keV)	Polycarbonate		High Density Polyethylene		Nylon	
	Fraction of Mean Free Path	Observed Transmission Fraction	Fraction of Mean Free Path	Observed Transmission Fraction	Fraction of Mean Free Path	Observed Transmission Fraction
13.9	0.36	0.698 ±0.054	0.97	0.397 ±0.030	0.22	0.830 ±0.064
17.5	0.19	0.823 ±0.082	0.56	0.605 ±0.060	0.12	0.891 ±0.088
21.1	0.14	0.881 ±0.089	0.42	0.702 ±0.109	0.08	0.928 ±0.073
26.4	0.10	0.918 ±0.024	0.33	0.749 ±0.021	0.06	0.950 ±0.019
32.1	0.08	0.964 ±0.0099	0.28	0.8135 ±0.0073	0.05	0.9914 ±0.0053
59.6	0.06	0.9401 ±0.0070	0.23	0.7912 ±0.0060	0.03	0.9699 ±0.0068
661.9	0.03	0.9699 ±0.0048	0.11	0.8891 ±0.0045	0.02	0.9887 ±0.0040

| Energy (keV)	Glass		Delrin		Rubber		
	Fraction of Mean Free Path	Observed Transmission Fraction	Fraction of Mean Free Path	Observed Transmission Fraction	Fraction of Mean Free Path Assumed Sulfur Composition	Fraction of Mean Free Path Assumed Silicon Composition	Observed Transmission Fraction
13.9	2.49	0.0669 ±0.0051	0.34	0.739 ±0.056	1.84	0.73	0.176 ±0.014
17.5	1.20	0.273 ±0.027	0.17	0.828 ±0.082	0.91	0.36	0.411 ±0.041
21.1	0.73	0.480 ±0.038	0.12	0.890 ±0.071	0.55	0.23	0.609 ±0.049
26.4	0.40	0.735 ±0.015	0.08	0.9553 ±0.019	0.31	0.14	0.795 ±0.016
32.1	0.24	0.7989 ±0.0042	0.06	0.9903 ±0.0053	0.10	0.10	0.8660 ±0.0046
59.6	0.08	0.9267 ±0.0064	0.05	0.9670 ±0.0068	0.07	0.05	0.9413 ±0.0066
661.9	0.02	0.9759 ±0.0039	0.02	0.9864 ±0.0040	0.03	0.02	0.9812 ±0.0040

MATHEMATICAL BASIS

All modeling was done using ISOCS/LabSOCS version 4.2 software. Each modeled geometry followed a similar format. This consisted of the circular plane geometry with the active source area being modeled as a near-point geometry located 7 cm on the vertical axis from the detector endcap. The attenuating material is modeled with the software's generic absorber, an infinitely wide sheet, with appropriate material thickness and density. Each attenuating material was custom defined based on best knowledge of the material composition. For each test material, two geometry files are created: one with and one without the generic absorber in place. The ISOCS transmission fraction is calculated by taking the ratio of the efficiency results at each energy for each geometry.

To determine the uncertainty in the software's transmission value, we used the documented uncertainties in the photon cross section values and the uncertainties in the

material's thickness and density. Correlations in the calculations of these uncertainties are identified and taken into account.

RESULTS AND DISCUSSION

In Figure 3 and Table 3, we present a comparison of the modeled transmission and the observed transmissions. For each material, the ratio of the transmissions is shown, such that a value of 1 indicates perfect agreement between modeled and observed results.
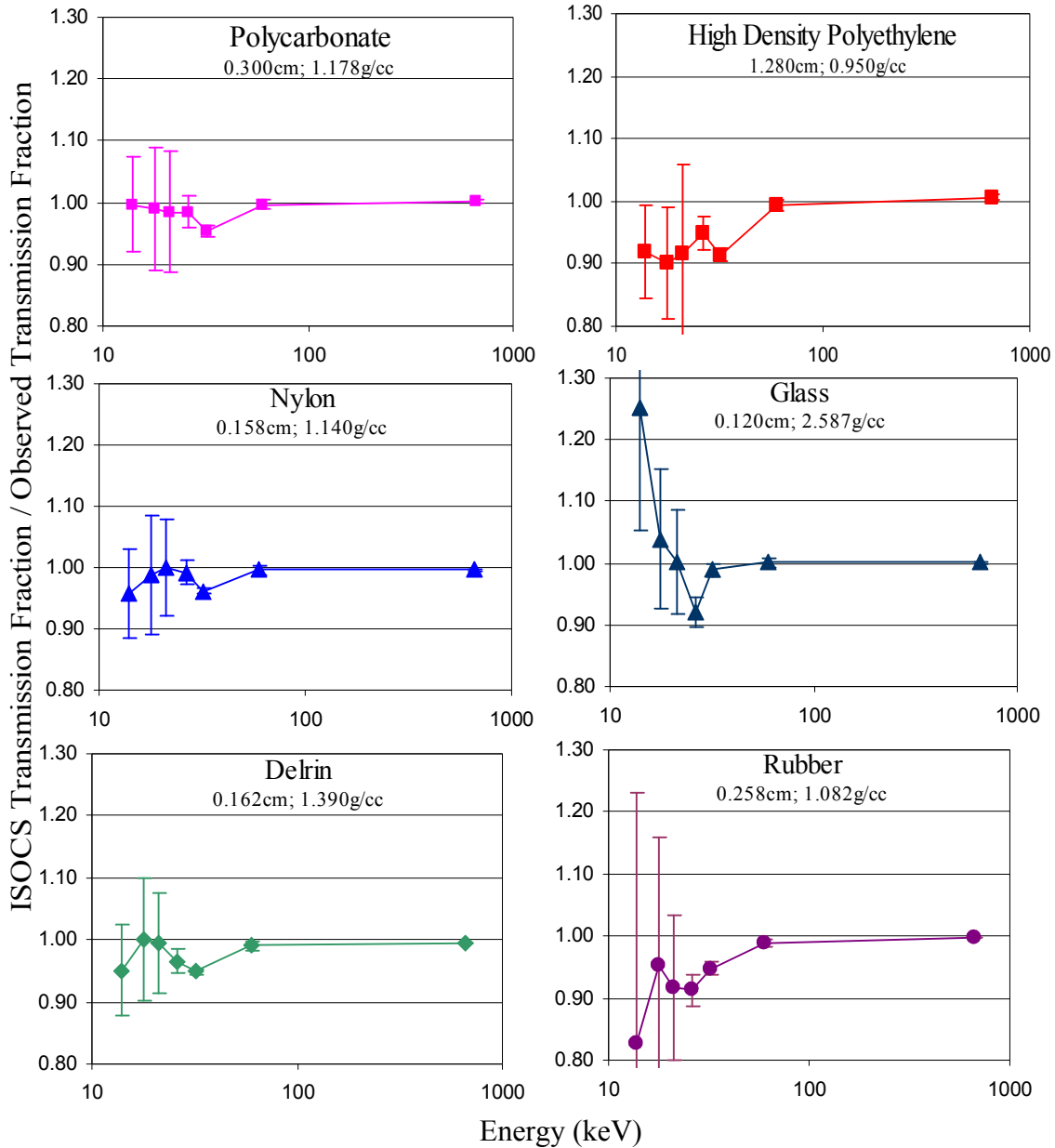
Figure 3 Comparison of modeled and observed transmission for different materials. Chemical compositions, densities, and thicknesses of the materials used are listed in Table 1. Rubber here is modeled as a sulfur-based synthetic compound. Error bars are a propagation of the absolute measured uncertainty at one standard deviation and the calculated modeling uncertainty specific to this experiment.

Error bars show a propagation of the modeled uncertainties, as described above, and the measurement uncertainties, which include statistical uncertainties and systematic fitting uncertainties. For the less-attenuating materials of the geometries studied, the majority of the error contribution is from counting statistics. The contribution to the final uncertainty from the uncertainty in the mass attenuation coefficient becomes magnified by the increasing thickness or density for a material and is therefore a more significant effect in circumstances of greater attenuation.

Table 3 Comparison of modeled to observed transmissions for different materials. Presented is the ratio of the calculated transmission fraction from the model to the observed transmission fraction from the measurement for each material at the indicated energies. Uncertainties listed are at one standard deviation and include measurement statistical and peak fitting accuracies as well as modeling uncertainties.

Energy (keV)	Polycarbonate		High Density Polyethylene		Nylon	
13.9	0.996	±0.077	0.919	±0.074	0.957	±0.074
17.8	0.990	±0.098	0.902	±0.090	0.989	±0.098
21.2	0.985	±0.099	0.916	±0.142	1.000	±0.080
26.3	0.984	±0.026	0.949	±0.028	0.9917	±0.020
32	0.9538	±0.0098	0.915	±0.010	0.9618	±0.0054
59.5	0.9971	±0.0074	0.993	±0.0091	0.9957	±0.0070
661.7	1.0010	±0.0049	1.0062	±0.0056	0.9956	±0.0041
Energy (keV)	Glass		Delrin		Rubber	
13.9	1.25	±0.19	0.951	±0.074	0.826	±0.40
17.8	1.04	±0.11	1.000	±0.099	0.954	±0.21
21.2	1.002	±0.085	0.994	±0.080	0.917	±0.12
26.3	0.921	±0.023	0.965	±0.020	0.912	±0.026
32	0.989	±0.010	0.9484	±0.0054	0.948	±0.0094
59.5	1.0013	±0.0072	0.9906	±0.0070	0.989	±0.0072
661.7	1.0007	±0.0040	0.9944	±0.0041	0.997	±0.0041

Glass exhibits the largest range of mean free paths in this set of materials and includes elements Si, Na, Ca, Mg, and Al in its chemical composition. At 13.9 keV, the model indicates a transmission of 25% (±19% 1sd) greater than observed. However, the true composition of this glass is not known and there is a large sensitivity of the transmission factor to the material composition of the modeled material. If we use 6.4% calcium dioxide by mass for the modeled material composition of glass, rather than 5.4%, there is a 6% difference in the calculated transmission fraction. Furthermore, 90% of the gamma-rays are absorbed at this energy, and peak shapes have become distorted due to small angle scatter. This results in a large degree of uncertainty of the measured value. At 17 keV, representing just over 1 mean free path and at about 30% transmission rates, agreement is within 5%.

For all other materials, at energies 662 keV and 59.5 keV, agreement is within 1%, and in the energy range 13.9 to 32 keV, modeled transmission values agree to within 10% of the observed transmission.

CONCLUSIONS

In this study we measured the gamma-ray transmission through a set of common low Z container and matrix materials. This dataset includes energies ranging from 13 keV to 662 keV and spans attenuating path lengths from 0.02 to 2.49 mean free paths. We modeled these geometries using Canberra's ISOCS/LabSOCS software and compared the modeled transmissions to the measured transmissions. We found agreement within 1% for all materials at energies greater than 45 keV. For energies less than 45 keV down to 13.9 keV, we reproduce measured transmission fractions to within 10%, with the exception of glass material at 13.9 keV, which is 25% (619% at one standard deviation). We have demonstrated the accuracy of the software's transmission correction factors, which are utilized in determination of absolute efficiencies. Overall, we have demonstrated that mathematical calibrations represent a viable alternative to source-based calibrations for quantification of efficiency at energies less than 45 keV.

REFERENCES

1. "*Calibration of Germanium Detectors for In-Situ Gamma-ray Measurements*", N42.28-2002 American National Standards Institute, Inc., 1430 Broadway, New York 10018.
2. "*A Good Practice Guide for the use of Modelling Codes in Non Destructive Assay of Nuclear Materials*", ESARDA Bulletin No. 42 (November 2009) 26.
3. R. Venkataraman, F. Bronson, V. Atrashkevich, B.M. Young, and M. Field, *Validation of in-situ object counting system (ISOCS) mathematical efficiency calibration software*, Nucl. Instr. and Meth. A 422 (1999) 450.
4. W.F. Mueller, F. Bronson, M. Field, K. Morris, D. Nakazawa, R. Venkataraman, V. Atrashkevich, "*Challenges and techniques to effectively characterize the efficiency of broad-energy germanium detectors at energies less than 45 keV.*", J. Radioanal. Nucl. Chem. 282 (2009) 217.
5. H. Zhu, R. Venkataraman, W. Mueller, J. Lamontagne, F. Bronson, K. Morris, and A. Berlizov, "*X-ray true coincidence summing correction in Genie 2000*", Appl. Rad. and Isotop. 67 (2009) 696.
6. H. Zhu, K. Morris, W. Mueller, M. Field, R. Venkataraman, J. Lamontagne, F. Bronson, and A. Berlizov, "*Validation of true coincidence summing correction in Genie 2000 V3.2*", J. Radioanal. Nucl. Chem. 282 (2009) 205.
7. D.E. Cullen, M.H. Chen, J.H. Hubbell, S.T. Perkins, E.F. Plechaty, J.A. Rathkopf, and J.H. Scofield, "*Tables and Graphs of Photon Interaction Cross Sections from 10 eV to 100 GeV Derived from the LLNL Evaluated Photon Data Library (EPDL)*", Lawrence Livermore National Laboratory report UCRL-50400, Vol. 6, Rev. 4, Part A: Z = 1 to 50 and Part B: Z = 51 to 100 (1989).
8. M.C. Lepy, J. Plagnard, and L. Ferreux, "*Measurement of ^{241}Am L X-ray emission probabilities.*" Appl. Rad. and Isot. 66 (2008) 715.